CdTe films electrodeposited from chlorine-containing solutions

1999 J. Phys.: Condens. Matter 11 9115

(http://iopscience.iop.org/0953-8984/11/46/313)

J. Phys.: Condens. Matter **11** (1999) 9115–9126. Printed in the UK PII: S0953-8984(99)03388-3

CdTe films electrodeposited from chlorine-containing solutions

A E Rakhshani

Physics Department, College of Science, Kuwait University, PO Box 5969, Safat 13060, Kuwait

E-mail: rakhshani@kuc01.kuniv.edu.kw

Received 13 April 1999

Abstract. The diffusion-controlled electrodeposition process of cadmium telluride from chlorine-containing solutions of $CdSO_4$ and the films' structure and electrical properties are studied. The effect of deposition at different temperatures (25–85 °C) and at different cathode potentials (−580 to −610 mV, versus Ag/AgCl) on the films' structure is investigated.

Photo-induced current transient spectroscopy of bandgap energy levels has revealed the presence of a few shallow hole traps, which do not exist in films prepared from Cl-free solutions, and, thus, are related to chlorine/structural defect complexes.

Due to the presence of the shallow hole traps, the electrical properties of these films and the charge transport mechanism in Au–CdTe devices are remarkably different from those in films deposited from Cl-free solutions.

The spectral response of the photocurrent reveals a direct bandgap energy of 1.460 eV at 300 K, which is about 30 meV smaller than the bandgap in films prepared from Cl-free solutions.

1. Introduction

Cadmium telluride is an important II–VI semiconductor with a variety of applications including photovoltaic ones. Fabrication of CdTe-based solar cells has shown promising results [1–3]. These cells can be prepared by different techniques including electrodeposition [4, 5]. The conversion efficiency of electrodeposited cells has reached 14% [6] and is anticipated to improve further, if the films' electrical and optoelectrical properties and, consequently, their photovoltaic properties can be controlled more closely. These properties and the effectiveness of extrinsic doping are influenced by the deep energy levels, which are associated with native defects, impurities and their complexes [7, 8].

Electrodeposition of CdTe for the fabrication of solar cells has been performed initially from an aqueous solution containing Cd^{2+}, SO_4^{2-} and $HTeO_2^+$, as described by Basol [4]. Films deposited from this solution are n-type and their physical properties have been studied in the past. The result of our studies on these films which include optical properties [9], electrical properties [10] and the spectrum of deep energy levels [11] have been reported lately.

Electrodeposition of CdTe from the solution quoted above but with an additional concentration of chlorine ions [5, 12–14] or from $CdCl_2$ solutions [15] has been reported. The reason for adding chlorine into the plating solution is due to the better performance of solar cells made from these films, though the effect of chlorine on the films characteristics has not been discussed explicitly in any of these publications.

In this work we report on the electrodeposition characteristics, the structure and electrical properties of films deposited from chlorine-containing solutions. It is shown that the spectrum of bandgap energy levels and consequently the charge transport mechanism in these films are

0953-8984/99/469115+12$30.00

remarkably different from those in films prepared from Cl-free solutions. The present films exhibit slight p-type behaviour, in contrast to the n-type behaviour of previous films and, thus, should be more suitable for the fabrication of p-CdTe/n-CdS heterojunction solar cells. The conductivity type was determined from the type of band bending at the Au/CdTe contact which, in turn, was established from the easy direction of current under illumination.

2. Experimental details

Electrodeposition of CdTe on flexible substrates (0.05 mm thick stainless steel) was performed from a $CdSO_4$ (1 M) bath with pH = 2. The deposition potential was in the range −580 mV to −600 mV with respect to a silver/saturated silver chloride standard electrode. Deposition was performed in the temperature range of 25–86 °C. Tellurium dioxide was added to the solution to form $HTeO_2^+$ (20–200 μM) and chlorine was added as $CdCl_2$ (0.06 M) after the solution had been electropurified for 10–15 h. The details of electrodeposition and the measurement of film thickness can be found elsewhere [4, 5, 9, 16].

The structure and composition of films were determined by the x-ray diffraction (XRD) method, using a Siemens diffractometer model D500 (Cu Kα: 0.154 06 nm), scanning electron microscopy (SEM) and the energy dispersive analysis of x-rays (EDAX), using a JEOL (JSM-6300) electron microscope.

For current–voltage (I–V) measurements and the study of deep energy levels by photo-induced current transient spectroscopy (PICTS), semi-transparent circular gold electrodes (14 nm thickness, 2 mm diameter) were evaporated on CdTe. The positive voltage bias refers to the gold electrode being at a potential higher than the substrate. A computer-controlled setup consisting of Keithley 236 source/measure unit, Keithley 428 current amplifier, Sciencetech 9050 monochromator and Stanford SR530 lock-in amplifier was used for the measurement of I–V characteristics and the photocurrent spectral response.

The setup used for PICTS measurements is described elsewhere [11]. PICTS is a suitable technique for studying the trapping levels in high resistivity materials [17–19]. In brief, the transient photocurrent was measured at different temperatures, and double-gate PICTS signals were generated. Light pulses (1 ms duration) from a light-emitting diode (peak intensity at 637 nm) were used for excitation. Illumination (through the gold electrode) at this wavelength generates electron–hole pairs just beneath the Au/CdTe interface. The selection of bias polarity allowed the injection of either holes or electrons into the bulk of the film for trapping. This technique has been applied successfully to distinguish between the hole and the electron traps [11]. The double-gate PICTS signal is the difference between the value of the transient current at two selected delay times. The time origin is taken at the onset of the exponential decay in the transient current. The PICTS signal peaks at a temperature, T_m, at which the emission rate e_m of the trapped charge is obtainable from the selected time gates. By varying e_m through the two time gates, T_m varies accordingly in order to satisfy [11]:

$$e_m = A\sigma T_m^2 \exp(-E/kT_m). \tag{1}$$

Above, k is the Boltzmann constant, $A = 1.35 \times 10^{24}$ s^{-1} m^{-2} K^{-2} for emission of trapped electrons into the conduction band and $A = 1.07 \times 10^{25}$ s^{-1} m^{-2} K^{-2} for emission of trapped holes into the valence band [11]. E and σ are, respectively, the apparent energy and capture cross section of the trap which can be determined from an Arrhenius plot of $Y = e_m/T_m^2$ against $X = 1000/T_m$.

3. Results and discussion

3.1. Deposition characteristics

Electrodeposition of CdTe from Cl-containing $CdSO_4$ solutions is a diffusion-controlled process. Similar to deposition from Cl-free solutions, the current density, J, decays with time, t, as [16]:

$$J = J_0 \exp(-t/\tau) \tag{2}$$

where $J_0 = enD(C_0 - C_s)/\delta$ and $\tau = \delta V/AD$. C_s and C_0 are, respectively, the concentration of $HTeO_2^+$ at the substrate surface and in the bulk of solution at $t = 0$. δ is the thickness of the diffusion layer across which $HTeO_2^+$ concentration decreases uniformly from its bulk value to C_s; δ is in the range of a few 10 μm with rapid stirring of the solution. e is the electronic charge and n is the number of electrons needed for depletion of one Te atom from solution. For stoichiometric deposition of CdTe, n is close to 6 since for each Te atom one Cd atom is also depleted through a six-electron transfer process [16]. Using the Faraday law of deposition, the value of n can be determined experimentally from the mass of the film and the total electric charge passed during deposition. V is the solution volume, A is the deposition area and D is the diffusion constant for $HTeO_2^+$ cations.

Deposition from Cl-free solutions follows equation (2) for a deposition potential in the range -550 mV to -600 mV and a solution temperature in the range 60 °C to 86 °C. The experimental value for n is in the range 5.8 to 7. At lower temperatures, n increases appreciably (e.g. $n = 14.4$ at 38 °C for deposition potential -600 mV) and equation (2) is not obeyed (unless at the tail region of the current decay) indicating that deposition is not entirely controlled by diffusion of $HTeO_2^+$ ions. At these low temperatures, only deposition potentials close to -600 mV yield reasonably uniform and adherent films.

Deposition from Cl-containing solutions was studied for plating potentials in the range -580 mV to -610 mV and solution temperatures in the range 25–85 °C. The deposition current density against time for different plating potentials at 85 °C is shown in figure 1. The validity of equation (2) is evident from the linear semilogarithmic plots. The curve corresponding to -590 mV measures an initial current density J_0 less than those for the other plots. This is due to a lower initial concentration of $HTeO_2^+$ ions in solution ($C_0 \approx 81$ μM) for this deposition compared to 164–178 μM for the other three curves.

From the measurement of J_0 and the slope $1/\tau$, the value of C_s was determined as $\approx$10 μM. For this, C_0 was calculated from the mass of TeO_2 added the solution and n was obtained from the mass of deposit and the electric charge involved (area under J–t plot).

The concentration of $HTeO_2^+$ remaining in solution after a film is deposited is always measured as less than the expected value obtainable from the initial concentration of $HTeO_2^+$ in the solution and the amount of Te deposited out into the film. This is the case only when the solution contains chlorine. This excess loss of $HTeO_2^+$ from solution is in a range to account for the deposition of one excess Te for each two to three molecules of CdTe. Since XRD and EDAX results did not show the presence of excess Te in films, the excessive loss is probably due to the passivation of $HTeO_2^+$ ions through a reaction involving chlorine. The results revealed that the concentration of the passivated $HTeO_2^+$ ions increases with the deposition time.

Deposition in the range -580 to -610 mV and at some selected temperatures revealed that, similar to the case for Cl-free solutions, n increases as temperature is reduced; n varies in the ranges 6.0–6.5, 7.0–9.5, 10.5–11.5 and 35–43, for deposition at 85, 63, 40 and 25 °C, respectively. Films prepared at 40 and 25 °C were uniform only when the deposition potential was in the vicinity of -600 to -610 mV.

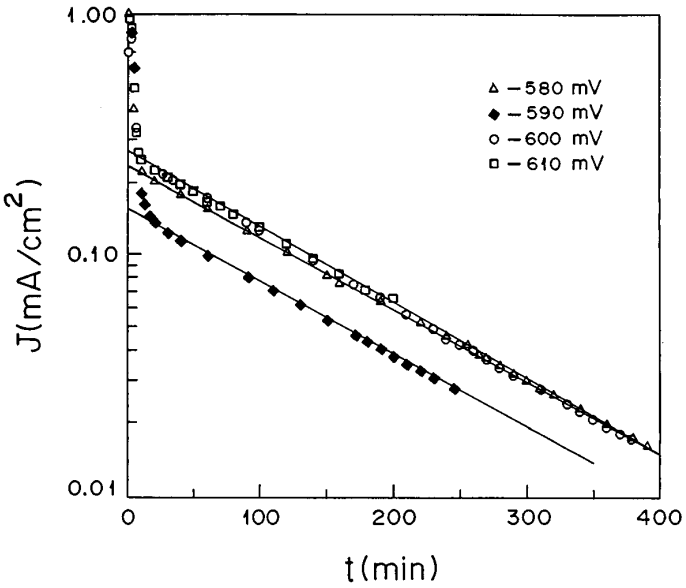

Figure 1. Deposition current density against time for four samples prepared at different deposition potentials from a solution of volume 750 ml at 85 °C. The initial concentration of $HTeO_2^+$ in the solution was about 81 μM for the lower plot (film thickness 0.68 μm, area 33.3 cm^2) and 164–178 μM for the other curves corresponding to film thicknesses in the range 1.3–1.4 μm and deposition areas in the range 34–39 cm^2.

3.2. Film structure

The structure of films prepared at different potentials and temperatures, in the ranges discussed above, was studied. Independent of temperature and potential, grains are highly oriented along their (111) planes parallel to the substrate surface. The EDAX and XRD studies revealed that all samples were stoichiometric. Peaks related to metallic Te or Cd were not observed in any of the XRD spectra. Table 1 summarizes the result of measurements on the full width at half maximum (FWHM) of the (111) peak, and the average size of grains in these films. The average sizes of grains were estimated from SEM micrographs and also from the FWHM values using the Scherrer formula [20]

$$D' = k\lambda/B\cos\theta. \tag{3}$$

D' is the grain size, B is the FWHM value, λ is the wavelength of the x-rays used, θ is the diffraction angle corresponding to the XRD peak and k is the Scherrer constant (0.94) which depends on the crystallite shape. For calculation of D', we took $k = 1$, in line with widespread practice. It should be noted that though equation (3) gives an approximate value for the grain size it can be used safely for relative measurements.

The results of SEM studies revealed that deposition at 25 °C yields grains with an average size much below 100 nm, which thus, could not be seen in the SEM micrographs. Deposition at 40 °C yields grains with a size ≈100 nm. Slightly larger grains (100–300 nm) can be obtained at 63 °C. At a higher deposition temperature (85 °C), many small grains (≈100 nm) cluster to form large domains, as figure 2 shows. These domains look like large grains (a fraction of 1 μm) under low SEM magnifications. The formation of domains was also observed in the absence of chlorine in solution and, thus, is not related to the effect of chlorine. The grain-cluster structure has also been observed in CdTe films deposited by sputtering [21].

Table 1. The full width at half maximum (FWHM) of the (111) XRD peak, the grain size estimated from the Scherrer equation, D', and from SEM measurements, D, for a film of thickness d, deposited at temperature T and potential V.

Sample	Thickness (μm)	T (°C)	V (mV)	FWHM (°)	D' (nm)	D (nm)
1 S26	0.36	25	−580	0.280	32	
2 S28	—	25	−610	0.428	21	
3 S29	0.72	40	−610	0.213	42	100
4 S34	1.1	63	−580	0.237	38	100–150
5 S32	1.6	63	−590	0.179	50	300
6 S31	0.8	63	−610	0.206	44	200
7 S38	1.3	85	−580	0.205	44	100 (domains 500)
8 S44	1.7	85	−590	0.193	47	as above
9 S42	1.4	85	−600	0.182	49	as above
10 S43	1.3	85	−610	0.195	46	smaller domains

The grain sizes calculated from FWHM values in table 1 are in the range of 40–50 nm which are two to four times smaller than the sizes obtained from SEM studies. Such a difference has also been observed in evaporated films of CdTe and is explained by the fact that each grain observed by SEM is a cluster of submacroscopic crystallites [22]. This implies that the grains in figure 2(a) are possibly composed of smaller crystallites that are not observable.

The data in table 1 reveal that the grain size does not change appreciably with deposition temperature in the range 40–85 °C. However, deposition at room temperature yields smaller grains. For films deposited at 63 °C and 85 °C, the grain size increases as deposition potential is reduced from −580 mV to −600 mV; a similar effect has been reported for films deposited from solutions without chlorine [23]. Further reduction of potential to −610 mV decreases the grain sizes. This is probably due to the effect of excess Cd in films. Excess Cd can be deposited at −610 mV but apparently not to the extent detectable by XRD and EDAX measurements. Films deposited at 85 °C and −610 mV show a lower resistivity (a few orders of magnitude) and negligible photoconductivity, possibly as a result of having excess cadmium.

The lattice constants were calculated from the angular positions of the (111) peaks for samples listed in table 1. The lattice constants for films deposited at the same temperature but at different potentials were averaged. The average value for the lattice constant was 0.6507 nm, 0.6471 nm, 0.6469 nm and 0.6484 nm for films deposited at 85 °C, 63 °C, 40 °C and 25 °C, respectively. The overall average for the ten films in table 1 is, however, 0.6474 nm, which is very close to 0.6481 nm (JCPDS diffraction files) for powder CdTe [20] and 0.6479 nm for films electrodeposited from $CdCl_2$ solutions [15]. Since powder samples are probably stress free, the fact that the lattice constant along the [111] direction (normal to the film plane) is greater or smaller than that of the powder samples indicates that there is compressive or tensile stress in the film plane, respectively. From the above data one may conclude that the residual stress along the film plane is negligible for films deposited at 25 °C. Films deposited in the 40–60 °C range have tensile residual stress, while films with larger lattice constants deposited at 85 °C have compressive residual stress. The compressive stress in the latter films is likely related to the presence of domains in films prepared at 85 °C. The domains consist of clustered grains, as shown in figure 2.

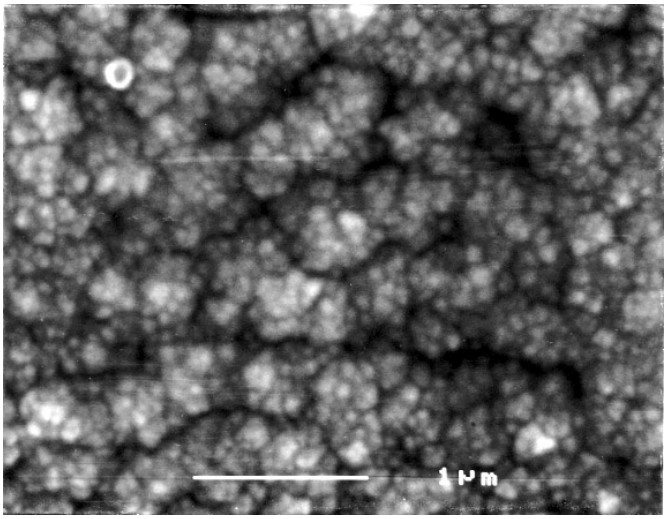

(a)

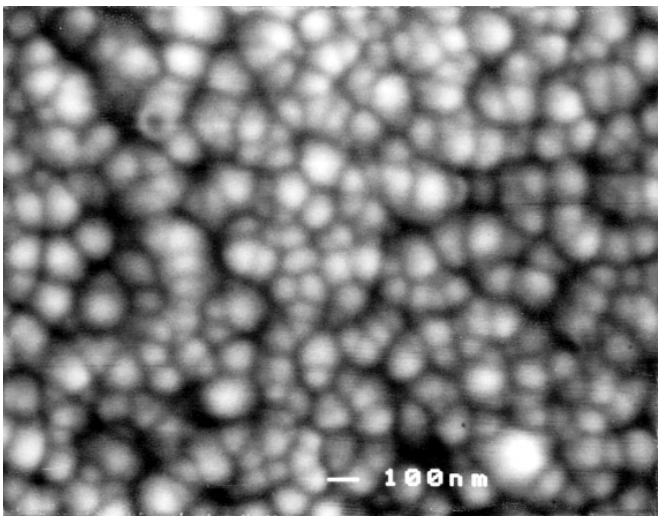

(b)

Figure 2. SEM views from the surface of CdTe films deposited at 85 °C (a) and at 63 °C (b); deposition potential is −580 mV for both.

3.3. Bandgap energy levels

The spectrum of deep and shallow trapping levels and the I–V characteristics in films deposited at different temperatures and at different deposition potentials were studied and the results will be reported. Here we report the typical characteristics for only one sample (S62), which was deposited at 85 °C and at −580 mV. Figure 3 shows the PICTS spectrum for sample S62. This spectrum was obtained during the first experiment done on this sample (run 1). The Arrhenius plots corresponding to peaks A and B which are shown in the inset measure two hole traps, 0.02 eV and 0.12 eV, above the valence band edge E_v. There are apparently other traps corresponding to other two peaks, occurring below ≈80 K and at about 340 K (peak

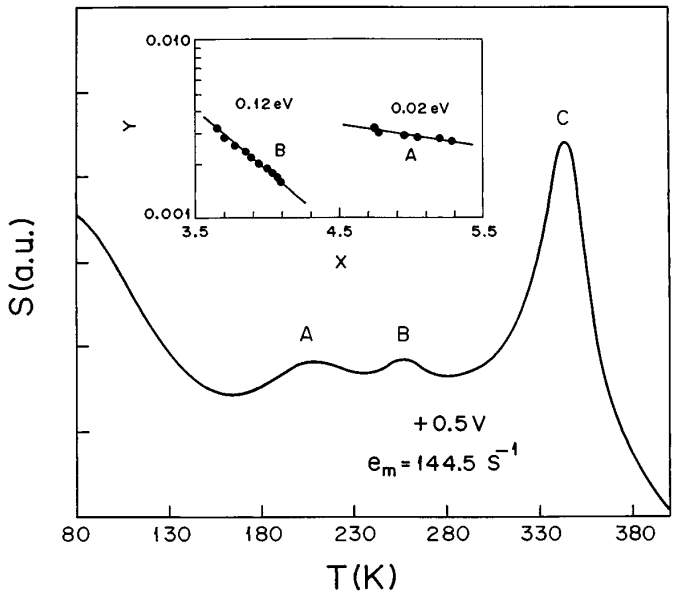

Figure 3. Double-gate PICTS spectrum (run 1) for sample S62 (0.91 μm) with a bias $V = +0.5$ V and an emission rate window $e_m = 144.5\ s^{-1}$. The Arrhenius plots of $Y = e_m^2/T_m$ ($s^{-2}\ K^{-1}$) against $X = 1000/T_m$ (K^{-1}) corresponding to peaks A and B are shown in the inset. The trap energies, 0.02 eV (A) and 0.12 eV (B), and their capture cross sections measured from these plots are listed in table 2.

C). The former was below the measurement limit and the latter did not move systematically with varying emission rate window. This behaviour of peak C is probably due to the changes occurring in the film properties at above room temperature. After temperature reached 400 K, the sample was cooled to 80 K and the second run of measurements was performed during the temperature rise. The result is presented in figure 4. Peak B becomes dominant while A and C are shown as shoulders. The new hole traps are located at 0.06, 0.23 and 0.30 eV above E_v. The PICTS measurement on the same sample but with a negative bias -1 V resulted in an electron trap, 0.54 eV below the conduction band edge E_c. The energy, capture cross section and the type of trap in this sample is listed in table 2. The assignment of traps to trace impurities, native defects and their complexes was done based on the numerous published data in the literature, including [8, 11, 24–29]. Peak A, in both runs, represents a shallow hole trap, probably due to a trace impurity such as Li, Na, P, N [8, 24], oxygen [26] or/and a complex defect like Te_i^{2-}/Cl_{Te}^{+} [27]. Peak B in the first run can be assigned to a trace impurity like Ag or to the complex defect V_{Cd}^{2-}/Cl_{Te}^{+} [8, 11, 24, 25]. Peak B in the second run represents a complex defect, or a grain boundary (GB) defect. Peak C in run 2 can be assigned to Au, Ag or, most likely, to a Cu trace impurity [8]. Copper can behave as an acceptor with ionization energy of 0.30–0.35 eV, by substitution into Cd sites [28, 29]. The result of our measurements on Cu-doped CdTe, electrodeposited from Cl-free solutions (not reported here) has revealed a distinct hole trap at $E_v + 0.30$ eV with $\sigma = 4 \times 10^{-21}$ cm^2. It has been demonstrated that Cu can also create complexes with native defects and/or chlorine, giving rise to a band of defect levels 0.11–0.23 eV above E_v, which leads to self-compensation of the material [28, 29]. The association of chlorine with this band of defects is supported by the fact that this defect band was detected only in the present samples but not in any of the samples deposited from Cl-free solutions [11].

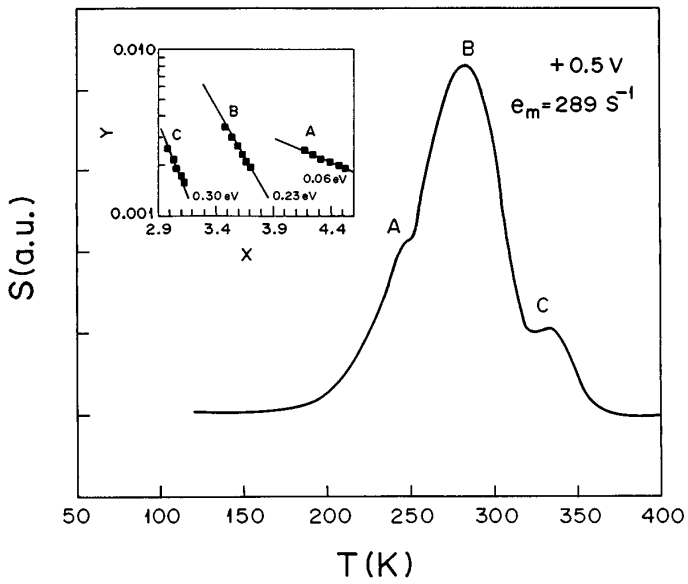

Figure 4. Double-gate PICTS spectrum (run 2) for sample S62; $V = +0.5$ V and $e_m = 289\ s^{-1}$. The Arrhenius plots of $Y = e_m^2/T_m$ ($s^{-2}\ K^{-1}$) against $X = 1000/T_m$ (K^{-1}) shown in the inset, correspond to hole traps with energies 0.06 eV (A), 0.23 eV (B) and 0.30 eV(C) above E_v. These values and the capture cross sections are listed in table 2.

Table 2. Electrical and deep level parameters for a 0.91 μm thick CdTe sample (S62) deposited at $V = -580$ mV and $T \approx 85\,^{\circ}$C. The concentration of chlorine in solution was 0.06 M. σ is the trap apparent capture cross section and E is its apparent ionization energy. The I–V parameters ϕ, n and m are, respectively, the barrier height, the ideality factor and the power factor. The type of trap (electron or hole) is denoted by e or h respectively. The bias used for PICTS measurements was +0.5 V in run 1 and run 2 and −1 V in run 3.

Run	ρ (Ω cm)	Forward bias[a]	I–V parameters	E (eV)	σ (cm^2)	Type	Assignment
1	1×10^5	negative	$m = 3/2$	$E_v + 0.02$	4.5×10^{-23}	h	Li, Na, P, N [8, 11], O [26],
2		negative		$E_v + 0.06$	1.4×10^{-22}	h	Te_i^{2-}/Cl_{Te}^{+} [27]
1				$E_v + 0.12$	1.9×10^{-21}	h	Ag, V_{cd}^{2-}/Cl_{Te}^{+} [11, 24, 25]
2				$E_v + 0.23$	1.4×10^{-19}	h	GB[b] complex defect [28, 29]
2				$E_v + 0.30$	3.1×10^{-19}	h	Cu [8, 28]
3		positive	$n = 1.37$, $\phi = 0.93$ eV	$E_c - 0.54$	5.7×10^{-17}	e	Cd_i^{2+} [11]

[a] Bias polarity for forward current.
[b] Grain-boundary defect.

Temperature cycling during PICTS measurement can induce changes in the deep-level spectrum as a result of structural changes, migration/activation of trace impurities and formation of complex defects.

The hole traps measured for sample S62 in both PICTS runs and also for many other samples are distinctly shallower than the hole traps in the n-type samples prepared from solutions in which chlorine was not added intentionally. For the latter samples, the ionization energy of the hole traps is greater than $E_v + 0.5$ eV and the Fermi level E_f is slightly above the intrinsic level E_i [11]. Apparently, due to the presence of shallow hole traps in sample S62,

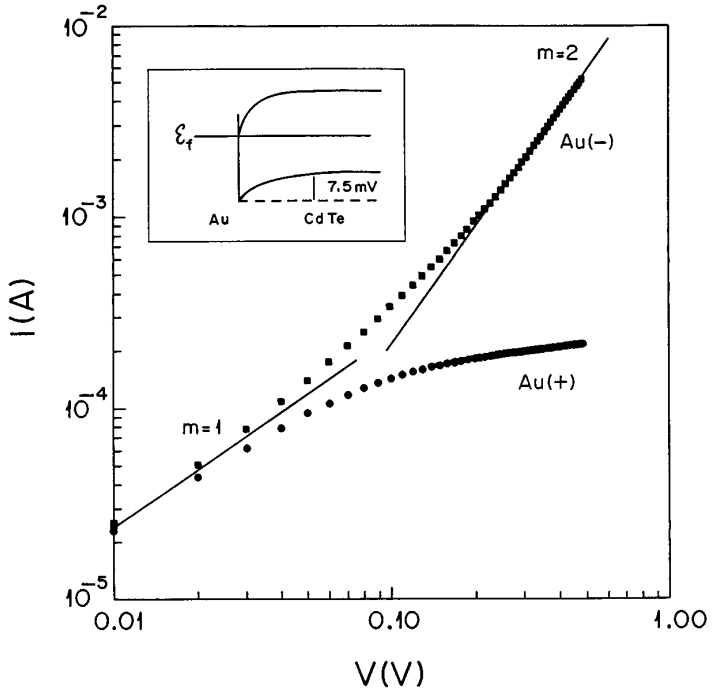

Figure 5. Current–voltage characteristics for a virgin device on sample S62. The I–V dependence, for negative biases, changes from ohmic at low biases to the power law $I \propto V^2$ at high biases. The inset shows the downward band bending of CdTe at the gold interface, corresponding to a flat band potential of 7.5 mV.

the Fermi level is situated below the Fermi level position in n-type samples. As a result, this sample showed p-type behaviour despite its relatively high resistivity. This was established from the downward band bending at the gold contact. The downward band bending, as shown in the inset of figure 5, was determined from the easy direction of the photocurrent. The flat-band potential was measured about 7.5 mV.

3.4. I–V characteristics

In the following discussions the back contact between CdTe and the substrate is taken to be ohmic. This is probably the case since in the initial stage of deposition, non-stoichiometric and, thus, highly defective monolayers are anticipated to form. Figure 5 shows the I–V characteristics in the dark, for a virgin device that had been cut from sample S62. The forward current corresponds to a negative bias that is in accordance with the downward band bending, established from photocurrent measurements. The forward current varies in proportion to V^m, indicating that the space-charge-limited current (SCLC) conduction is the dominant charge transport mechanism [30]. In the conventional SCLC, where conduction is controlled by discrete trapping levels, the power factor is $m = 2$, as is the case shown in figure 5 in the bias range $V > 0.2$ V. For another virgin device on this sample which was used for PICTS measurements (table 2), $m = 3/2$ was obtained. The result of measurements on many other samples revealed that for all samples with downward band bending and for which forward current corresponds to negative biases, the power factor m is either 2 or 3/2. When the carrier

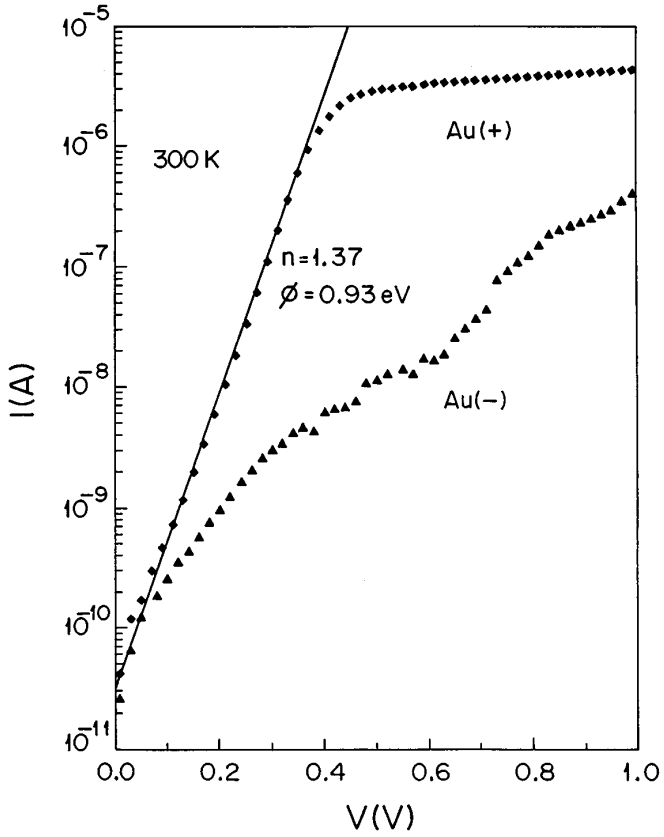

Figure 6. Current–voltage characteristics for the device of figure 5, after being heat treated in vacuum. The reverse current corresponding to negative biases was unstable. The fit of forward current to the diode equation gives an ideality factor $n = 1.37$ and a barrier height $\phi = 0.93$ eV.

drift mobility is field dependent, $m = 3/2$. This is the case normally at high fields when the drift velocity of warm carriers varies in proportion to the square root of the field [30]. The I–V plots for films prepared from Cl-containing solutions, but at different deposition potentials, have shown m values in the range 2.2–2.4 [14]. $m > 2$ is obtained in cases where there is a set of trapping levels with an exponential energy distribution [30].

The I–V characteristics for sample S62, after it was subjected to two temperature scans (80–400 K) in vacuum, are shown in figure 6. Similar to the case for n-type films prepared from Cl-free solutions, the forward current corresponds to positive biases, and obeys the Schottky barrier equation $I = I_0 \exp(qV/nkT)$, where the parameters have their usual meanings [10]. The fit of data to this equation gives an ideality factor $n = 1.37$ and a barrier height $\phi = 0.93$ eV. These parameters are identical to those for Au/CdTe devices fabricated with ohmic back contacts from Cl-free solutions [10]. The reverse current in figure 6 and in all other similar cases was unstable and relatively high. The change in the type of transport mechanism, which is due to the change in band bending, indicates that E_f has been shifted towards E_c as a result of heat treatment. This upward shift is also in accordance with the development of deeper hole traps (figure 4), and the electron trap (entry 6, table 2) with heat treatment in vacuum. The heat treatment of films in air (350–400 °C) and before the deposition of gold electrodes, also yields Schottky-barrier type I–V characteristics.

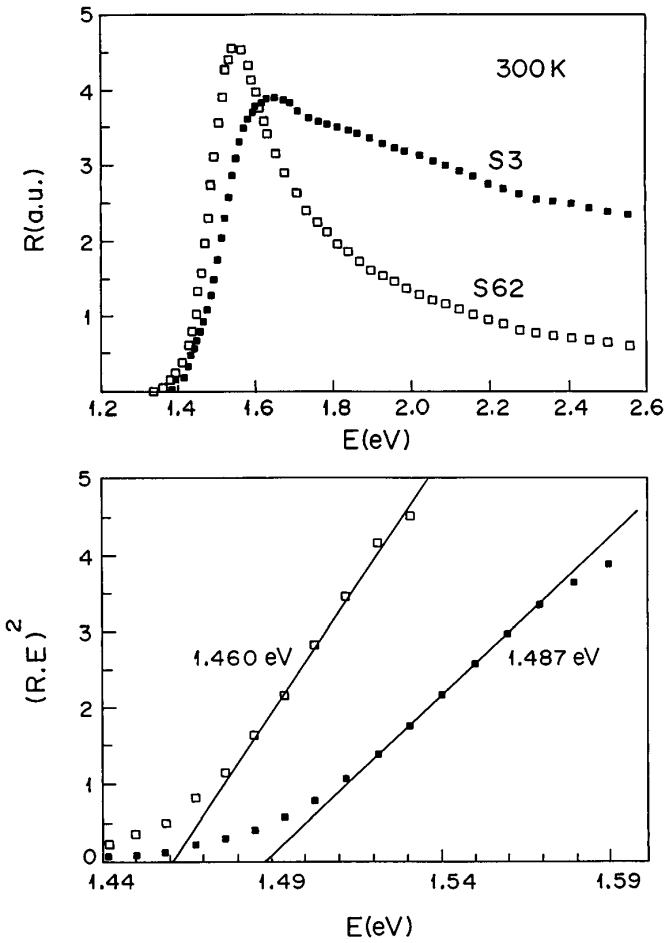

Figure 7. Quantum efficiency R, in arbitrary units, against the incident photon energy E for samples S62 and S3 (deposited from a Cl-free solution). For both, R was determined under short-circuit conditions. The direct optical transitions at 300 K are 1.460 eV and 1.487 eV, respectively.

3.5. Photocurrent spectral response

Figure 7 shows the spectral response for samples S62 and S3. The latter is a sample deposited at the same condition as for sample S62 (−580 mV, 65 °C) but from a Cl-free solution. In figure 7 the quantum efficiency R (photocurrent normalized to the photon flux at the Au/CdTe interface) is plotted in arbitrary units against the incident photon energy E. For photon energies close to the material bandgap, the optical absorption coefficient is not too high and, thus, R becomes proportional to it. In this range of photon energies, a plot of $(RE)^2$ against E is expected to yield a straight line with a horizontal intercept equal to the direct optical transition across the bandgap. Such plots are shown for both samples in figure 7. The direct transition in sample S62 (1.460 eV) is about 0.03 eV smaller than the direct transition (1.487 eV) in S3. This difference can be attributed to the presence of the 0.02 eV and 0.06 eV energy levels above E_v (see table 2) in sample S62. No such shallow levels could be detected in samples like S3, which were prepared from Cl-free solutions [11].

4. Conclusions

The presence of chlorine in solution has no apparent effect on the deposition mechanism that remains a diffusion-controlled process in a certain range of temperature and potential. However, the effect of chlorine is the partial passivation of $HTeO_2^+$ cations.

The presence of chlorine has no apparent effect on the morphology and structure of films. These properties depend on the deposition parameters such as temperature and potential.

Films deposited from Cl-containing solutions exhibit several shallow hole traps in their energy bandgap that do not exist in films deposited in the absence of chlorine. These traps lower the position of the Fermi level towards the valence band, causing a slight downward band bending at the Au/CdTe contact in contrast to upward band bending in films prepared from Cl-free solutions.

Acknowledgment

The support of Kuwait University under research project SP057 is gratefully acknowledged.

References

[1] Zweibel K, Chu T L and Chu S S 1993 *Advances in Solar Energy* vol 8, ed M Prince (Boulder: ASES) p 271
[2] Chu T L and Chu S S 1993 *Prog. Photovoltaics: Res. Appl.* **1** 31
[3] Britt J and Ferekides C 1993 *Appl. Phys. Lett.* **62** 2851
[4] Basol B M 1998 *Solar Cells* **23** 69
[5] Morris G C and Das S K 1992 *Int. J. Solar Energy* **12** 95
[6] Woodcock J M, Turner A K, Ozsan M E and Summers J G 1991 *Proc. 22nd IEEE Photovoltaic Spec. Conf. (Las Vegas)* (New York: IEEE) p 842
[7] Von Windhein J A and Cocivera M 1991 *J. Phys. Chem. Solids* **53** 31
[8] Zanio K 1978 *Semiconductors and Semimetals* vol 13, ed R K Willardson and A C Beer (New York: Academic) ch 3
[9] Rakhshani A E 1997 *J. Appl. Phys.* **81** 7988
[10] Rakhshani A E, Mathew X and Mathews N R 1998 *Phys. Status Solidi* a **168** 177
[11] Rakhshani A E 1998 *Phys. Status Solidi* a **169** 85
[12] Das S K and Morris G C 1993 *J. Appl. Phys.* **73** 782
[13] Morris G C, Tanner P G and Tottszer A 1991 *Mater. Forum* **15** 21
[14] Pal A, Dutta J, Bhattacharyya D, Chaudhuri S and Pal A K 1995 *Vacuum* **46** 147
[15] Qi B, Kim D, Williamson D L and Trefny J U 1996 *J. Electrochem. Soc.* **143** 517
[16] Rakhshani A E 1999 *Phys. Status Solidi* a **172** 379
[17] Balland J C, Zielinger J P, Nuguet C and Tapiero M 1986 *J. Phys. D: Appl. Phys.* **19** 57
[18] Brasil M J S P and Motisuke P 1990 *J. Appl. Phys.* **68** 3370
[19] Look D C 1983 *Semiconductor and Semimetals* vol 19, ed R K Willardson and A C Beer (New York: Academic) p 75
[20] Ashour A 1994 *J. Mater. Sci. Mater. Electron.* **5** 47
[21] Levi D H, Moutinho H R, Hasoon F S, Ahrenkiel R K, Kazmerski L L and Al-Jassim M M 1996 *AIP Conf. Proc.* vol 353, ed H S Ullal and C E Witt (New York: AIP) p 400
[22] Bonilla S and Dalchiele E A 1991 *Thin Solid Films* **204** 397
[23] Kampmann A, Cowache P, Mokili B, Lincot D and Vedel J 1995 *J. Crystal Growth* **146** 256
[24] Kuhn T A, Ossau W, Waag A, Bicknell-Tassius R N and Landwehr G 1992 *J. Crystal Growth* **117** 660
[25] Seto S, Tanaka A, Masa Y and Kawashima M 1992 *J. Crystal Growth* **117** 271
[26] Akimoto K, Okuyama H, Ikeda M and Mori Y 1992 *J. Crystal Growth* **117** 420
[27] Valdna V, Buschmann F and Mellikov E 1996 *J. Crystal Growth* **161** 164
[28] Samimi M, Biglari B, Hage-Ali M, Koebel J M and Siffert P 1987 *Phys. Status Solidi* a **100** 251
[29] Hage-Ali M, Yaacoub B, Mergui S, Samimi M, Biglari B and Siffert P 1991 *Appl. Surf. Sci.* **50** 377
[30] Lampert M A and Mark P 1970 *Current Injection in Solids* (New York: Academic)